KICS The Korean Institute of Communications and Information Sciences

Available online at www.sciencedirect.com

ScienceDirect

ICT Express 9 (2023) 69–75

www.elsevier.com/locate/icte

Searching similar weather maps using convolutional autoencoder and satellite images

Heewoong Ahn[a,1], Sunhwa Lee[b,1], Hanseok Ko[a], Meejoung Kim[c], Sung Won Han[b,*,2], Junhee Seok[a,2,*]

[a] *Department of Electrical Engineering, Korea University, Anam-dong, Seoul, 136-713, South Korea*
[b] *Department of Industrial Management Engineering, Korea University, Anam-dong, Seoul, 136-713, South Korea*
[c] *Research Institute for Information and Communication Technology, Korea University, Anam-dong, Seoul, 136-713, South Korea*

Received 31 August 2021; received in revised form 30 January 2022; accepted 25 March 2022
Available online 1 April 2022

Abstract

A weather forecaster predicts the weather by analyzing current weather map images generated by a satellite. In this analyzing process, the accuracy of the prediction depends highly on the forecaster's experience which is needed to recollect similar weather maps from the past. In an attempt to help forecasters to obtain empirical data and analyze the current weather status, this paper proposes a convolutional autoencoder model to find weather maps from the past that are similar to a current weather map by extracting the latent features of each image. To measure the similarity between each pair of images, metrics including mean squared error and structural similarity were used and case studies for searching similar satellite images were conducted and visualized. The paper also demonstrates that searching similar weather maps can be useful guidance to all forecasters when analyzing and predicting the weather.

Keywords: Deep learning; Weather map retrieval; Convolutional autoencoder; Unsupervised learning

1. Introduction

The weather has a direct impact on the environment and human activities [1] and it is closely related to various industries [2–8]. Either seasonal or daily weather changes determine crop yields which may result in the fluctuation in crop prices [7]. Heavy rains generate additional costs in distribution and service industries by restraining traffics and human activities [8]. Accurate weather forecasting is required not only in the meteorological field but also in most industries, as the weather is a major factor in policy decisions in those industries [9].

All the weather forecasters in the world report the weather for the next day several times each day. They analyze several weather factors such as air pressure, humidity, and temperature in a certain area. These weather factors can be observed and calculated by the satellites in space or measured by the meteorological stations on the surface. Among the weather factors from these two sources, the data from satellites are used to predict the overall weather in a wider area. Weather forecasters analyze the *geopotential height field* and the *temperature field* for each air pressure which is observed and recorded by the satellite to detect an atmospheric flow and predict probable weather. Most meteorological calculations are performed by the massive computing resource, but the final weather forecasts are established by a forecaster who analyzes the calculated and generated data. Because this task is performed multiple times a day, the accuracy of predictions depends on the experience of forecasters [10]. Therefore, if we find past weather maps similar to the current weather maps, it can help forecasters to analyze images efficiently.

In this study, we concentrate on searching similar past weather maps in the East Asian region centered on the Korean peninsula. Since the Korean Peninsula is affected by both the Asian continent in the east and the Pacific Ocean in the west, fluctuations in temperature and humidity vary depending on the atmospheric pressure. Therefore, we use the geopotential

* Co-corresponding author.
E-mail addresses: swhan@korea.ac.kr (S.W. Han), jseok14@korea.ac.kr (J. Seok).
[1] Both authors are contributed equally to this work.
[2] Both corresponding authors are contributed equally to this work.
Peer review under responsibility of The Korean Institute of Communications and Information Sciences (KICS).

https://doi.org/10.1016/j.icte.2022.03.013

Fig. 1. Structure of the convolutional autoencoder model.

height field images and the temperature field images by several air pressure levels observed from a satellite. If we find past weather maps of the geopotential height field and the temperature field whose structural distributions are similar, the forecaster can refer to those past weather data for the analysis.

2. Related works

2.1. Searching similar weather maps

Several studies for searching similar weather maps have been conducted to improve the analysis of forecasters and choosing a suitable method for extracting patterns from satellite images has been of most importance to searching similar weather maps. Kim et al. [11] flattened the satellite images into vectors and reduced the dimension of the vectors using principal component analysis. Similar weather maps were searched by comparing both distances between principal component vectors of satellite images and distances between pixel values of raw satellite images. Oh et al. [12] extracted patterns of satellite images using a Convolutional neural network (CNN) [13]. Latent features of images were generated by a CNN model which was pre-trained for face verification [14].

CNN in deep learning is the most powerful method to handle the imagery data. The filter of each layer in the neural network learns the hierarchical pattern in an image by capturing simple patterns and assembling more complex patterns [15–18]. More complex models have been derived from CNN for each purpose, and Google suggested the Inception Model [19] which won the ImageNet Large Scale Visual Recognition Competition (ILSVRC) in 2014. Inception solved the neural networks' overfitting problem by stacking several filters in each layer and made it possible to construct a deep layer [20,21].

M Tan and Q Le proposed EfficientNet [22] to efficiently optimize CNN-based deep network models within limited computing resources. EfficientNet which scales up all dimensions of depth, width, and resolution of a model with carefully balanced methods achieved both high efficiency and state-of-the-art accuracy on the CIFAR-100 dataset. The latent vectors the dimension of which is reduced using EfficientNet are also widely used in fine-tuning to boost the performance of a model.

Jonathan Masci et al. proposed a convolutional autoencoder (CAE) [23] in 2011 to extract features by unsupervised learning. The model uses the same input and output data and learns to reduce the dimension of the image and reconstruct the input image. The extracted features from these CNN-based models made it easier to solve most of the complex imagery problems [24]. (See Fig. 1.)

2.2. Metrics to measure similarities

After searching similar weather maps, metrics to measure the actual similarities between images are needed. The similarity of images can be measured by the mean squared error (MSE) of pixels in each image. MSE is a typical and general option for measuring performance in most studies. However, it focuses on how same the two images are, not how similar they are, which may estimate high MSE between two images that are similar in shape but different in scale [25].

Cosine similarity can be used to measure the similarity between two vectors. With images vectorized, the differences in direction of normalized vectors can be used to measure the similarities. Cosine similarity is a simple but powerful tool for measuring similarities between texts or any other multidimensional data. If we convert images into latent feature vectors, cosine similarity can be a metric to evaluate the similarity [26,27].

Zhou Wang proposed Structural Similarity (SSIM) to measure the similarity of images [28]. In this work, they adopted luminance masking terms and contrast masking terms, each considering the concept that image distortions vary in different brightness and different texture in the image [29–33]. The paper has provided a general context for evaluating perceptual quality measures and found strong adoption in the image processing field. SSIM can be a suitable metric to evaluate the similarity by comparing distributions of air pressure of satellite images.

Air near the surface flows down and away in a high-pressure system and air flows up and together in a low-pressure system. Such a flow of air has a great influence on the weather, so it is necessary to capture the relative difference in atmospheric pressure. In this study, we adopt CAE to extract features of all images and calculate the similarity between these vectorized features to search similar weather maps fast and efficiently. Then we verify the performance of CAE with several metrics such as MSE, cosine similarity, and SSIM, compared to that of the model based on Inception and EfficientNet models.

3. Materials and methods

3.1. Satellite weather map images

The type of satellite images used for learning is ERA-Interim, which is the latest global atmospheric reanalysis data produced by the European Centre for Medium-Range Weather Forecasts (ECMWF) [34,35]. All images have been selected from the East Asian region centered on the Korean peninsula and provided by the Korean Meteorological Administration (KMA). The region covers longitude from 107.604 to 159.149 and latitude from 17.400 to 159.149 53.502. The size of the image is 95 by 95, and all pixels are recorded in binary format with geopotential height (in meters) and temperature (in Celsius degrees) from 1000 hPa to 100 hPa atmospheric pressure at intervals of 100 hPa. The period of data for learning is 00, 06, 12, 18 UTC from January 1, 1979, to December 31, 2015 (see Table 1).

Table 1
Data specification.

Contents	Details
Region	East Asia(centered on the Korean peninsula)
Period	January 1, 1979 ∼ December 31, 2015
Time intervals	00 06 12 18 UTC
Pressure levels	1000 hPa ∼ 100 hPa at intervals of 100 hPa
Image size	95 by 95 pixels
Map parameters	geopotential heighttemperature

3.2. Deep learning methodology

For the deep learning method, a convolutional autoencoder (CAE) has been used. The hidden layers of CAE were under complete Encoder for feature extraction. The number of filters, the number of layers, and the filter size were hyper-parameters for learning. The number of filters for each of four encoding layers was 5, the size of the filter mask was 3 by 3, and the filter stride was 2 which were determined by minimizing the test error. Python 3.5, Tensorflow 1.8, and GTX 1080ti for GPU were used.

CAE reduced each image into a feature vector with 180 parameters and we connected 80 vectors to calculate the Euclidean distance of the entire feature vector for one day (See Fig. 2).

Pre-trained models of Inception-v1 and EfficientNet-b0 were compared with CAE. Both pre-trained models reduced each image into a vector with 1024 parameters.

3.3. Validation metrics

To measure the similarity between two images, we used four metrics as follows. The character x represents the weather map to be compared y represents the retrieved weather map similar to x weather map.

We calculated mean squared error (MSE) to compare the similarity between weather maps. MSE averages squared errors per pixel as follows:

$$MSE = \frac{1}{n}\sum_{i=1}^{n}(x_i - y_i)^2 \tag{1}$$

where x_i and y_i are a value of a pixel of a weather map. MSE of the root of MSE (RMSE) is also used in comparing similarities between the latent feature vectors extracted by neural network models.

Similar to MSE, relative error (RE) was also calculated to compare the relative similarity scaled by the mean value of weather map x. RE can determine the intuitive difference between two images especially when we investigate both geopotential height and temperature domain simultaneously.

$$RE = \sum_{i=1}^{n}|x_i - y_i| / \sum_{i=1}^{n} x_i \tag{2}$$

Metrics that calculate spatial errors such as cosine similarity and structural similarity (SSIM) can determine the similarities in terms of two-dimensional components. These errors can be useful when the overall pixel values differ while the flows of the air are similar.

$$Cosine\ similarity = x \cdot y / \|x\| \cdot \|y\| \tag{3}$$

$SSIM = 2(\mu_x\mu_y + C_1)(2\sigma_{xy} + C_2)/(\mu_x^2 + \mu_y^2 + C_1)\left(\sigma_x^2\sigma_y^2 + C_2\right)$, where μ_x, μ_y the mean of x and y, σ_x, σ_y the variance of x and y, σ_{xy} the covariance of x and y, $C_1 = (k_1 L)^2, C_2 = (k_2 L)^2$, $L = 2^{number\ of\ bits\ per\ pixel} - 1$,

$$k_1 = 0.01, k_2 = 0.03. \tag{4}$$

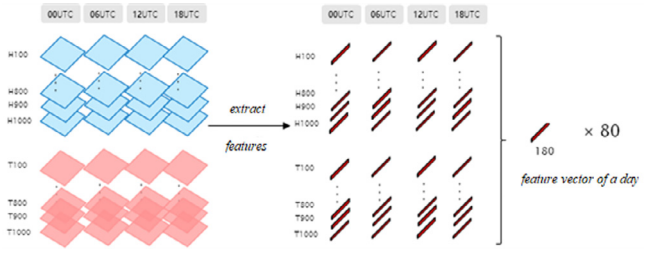

Fig. 2. Constructing feature vectors for one day.

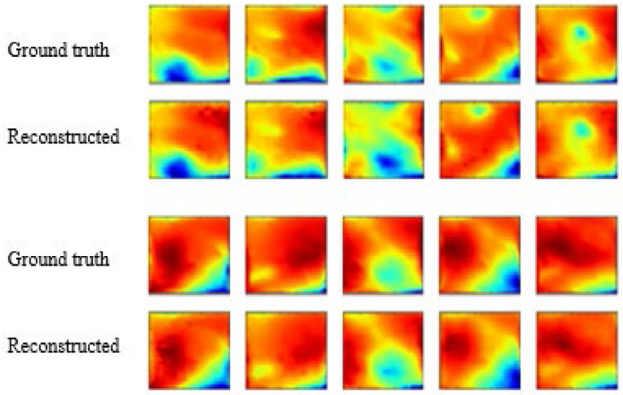

Fig. 3. 10 random sets of a ground truth image and a reconstructed image from test samples (geopotential heights in 900 hPa specifically) generated by convolutional autoencoder model.

4. Results

Each geopotential height and temperature data are composed of 10 images of air pressure from 1000 hPa to 100 hPa at intervals of 100 hPa for each date to be searched. For each day, we use data from four time zones: UTC 00, 06, 12, 18. That is, a total of 80 feature vectors are extracted with 10 times of geopotential height and temperature field for 4 time zones of 00, 06, 12, and 18 UTC a day. The period used for learning feature vectors is from 1979 to 2015, and the images of 2016 are extracted as a feature vector and compared with the dates of all the other years.

4.1. Reliability for convolutional autoencoder

In this study, since the feature vectors are compared without directly comparing the images, it is assumed that the similarity

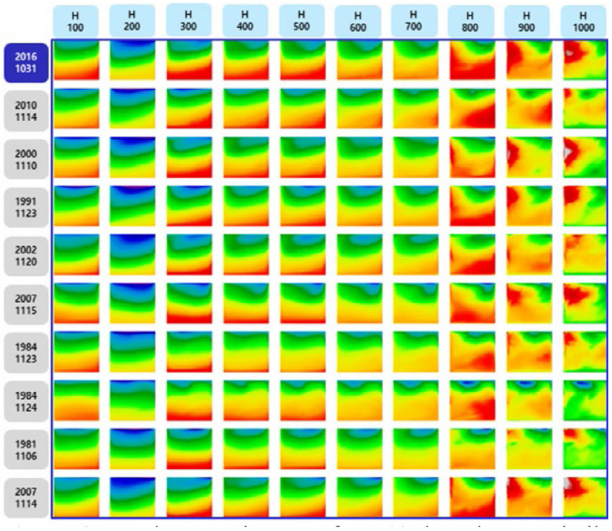

Fig. 4. Weather map images of top 10 days that are similar with Octover 30, 2016 00UTC searched by CAE model. The date list is ranked considering only geopotential height as an example.

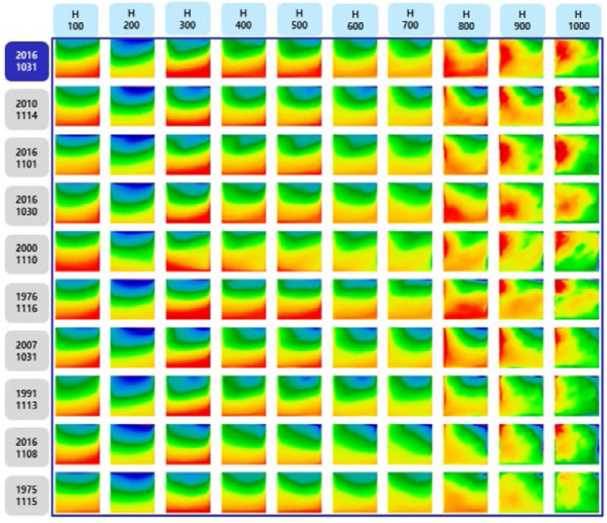

Fig. 5. Weather map images of top 10 days that are similar with Octover 30, 2016 00UTC searched by Inception-v1 model. The date list is ranked considering only geopotential height as an example.

of the feature vectors can reconstruct the original image from the compressed vector to show the similarity of the images. For this, we compare the reconstruction weather maps with the original weather maps in the test set, and the results of 10 randomly selected dates are shown in Fig. 3. The modified RMSE is calculated to show the difference between the original image and the restored image, and the modified RMSE is the RMSE between the two images divided by the average of pixels in the original image.

Weather maps in areas with low air pressure tend to have monotonous patterns, which may be insufficient to confirm that reconstruction is successful. For more accurate validation, we used a test set of weather maps of 900 hPa, which is just below the minimum pressure of the surface. The modified RMSE of

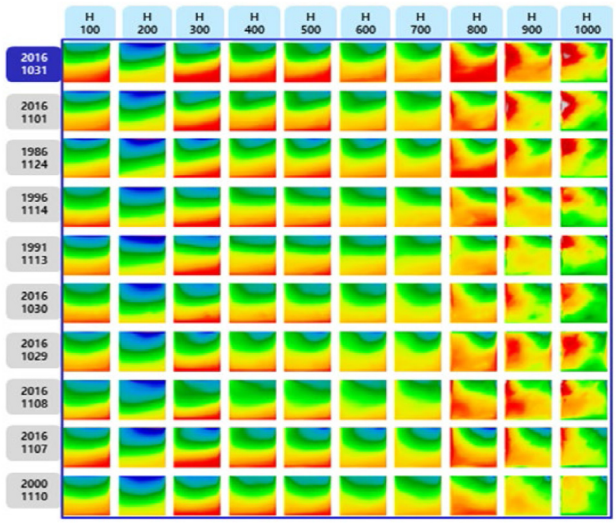

Fig. 6. Weather map images of top 10 days that are similar with Octover 30, 2016 00UTC searched by EfficientNet-b0 model. The date list is ranked considering only geopotential height as an example.

Table 2
Results of CAE model training.

	Training set	Test set
Period (year)	1979 ∼ 2015	2016
Modified RMSE	0.001	0.043

the test set is below 5%, and it is confirmed that the feature vector can be used for searching similar maps (see Table 2).

4.2. Comparison with pre-trained CNN model

To compare similarity metrics extracted from CAE, we used feature vectors extracted from Inception-v1 and Efficient-b0 models which are conventional CNN-based networks. Inception and EfficientNet model extracted the feature vectors of all the weather maps using pre-trained parameters to classify the images and compares them to find similar maps. For all dates, we extracted latent feature vectors using CAE and pre-trained models and listed similar dates by finding feature vectors nearest Euclidean distance to feature vectors of a specific date.

All four metrics were calculated to measure the performance of each model in the test set. The test set ranges from February 1, 2016, to November 30, 2016 (304 days). For each day in the test set, we listed the top 10 similar dates and calculated four metric scores. Then we averaged all the 304 median scores by metric of each day. The result is shown in Table 3. For cos similarity and structural similarity, the higher the score, the better the model performs. To show these two metric results intuitively by making the smaller score for the better performance, we modified both scores as follows:

$$(*\textit{modified metric score}) = 1 - (\textit{metric score}) \tag{5}$$

From Figs. 4 to 6 show 10 images from H100 to H1000 of 00UTC for each searched date using CAE, Inception, and EfficientNet when October 31, 2016, was the reference date.

Table 3
Four metrics for validation of CAE, Inception and EfficientNet model.

Model	MSE	RE	Cos similarity*	SSIM*
CAE	**1459.68**	**0.006319**	**1.6 e−5**	**3.4 e−5**
Inception	1686.71	0.006745	4.2e−5	4.5e−5
EfficientNet	1621.83	0.006702	3.8e−5	4.3e−5

Table 4
Relative errors (RE) of similar weather map lists by type of images that were used when searching similar weather maps.

Model	RE	RE_H	RE_T
CAE	**0.006319**	**0.006319**	**0.157968**
Inception	0.006745	0.006745	0.159041
EfficientNet	0.006702	0.006702	0.158724

As shown in the images of each Figs. 4 and 6, both CAE and pre-trained models showed high similarity to the top 10 weather maps. The date list by both methods is almost identical as shown in the example search results, but it is confirmed that CAE is more accurate as shown in Table 3, considering all MSE, SSIM, cosine similarity in average.

The performance of CAE and both pre-trained models can be considered to search similar weather patterns well while CAE showed the best performance. Considering the range of the value of raw images, the relative error (RE) by pixel of each model is significantly low which is 0.006319 in CAE, 0.006745 in the Inception model, and 0.006702 in the EfficientNet model as shown in Table 3. The geopotential height images were used when the RE score of each model was calculated because the geopotential images are considered to contribute more to searching overall similar weather images in real industries.

To determine the difference in the contribution of geopotential height and air pressure images, we searched another two lists of top similar 10 days of each date in the test period (February 1, 2016, to November 30, 2016) which are searched by considering only geopotential height images and only temperature images respectively. Then we calculated the relative error of each result (RE_H for geopotential height and RE_T for temperature respectively) as similarly as we calculated the relative error in Table 3. When searching similar weather maps only considering temperature images the RE_T was much higher as shown in Table 4. The values of RE_H of both models were the same as RE which indicate that geopotential height images were considered as the main factors when comparing each similar image set of a day.

CAE outperformed EfficientNet which generally delivers leading performances in several competitive problems. Although EfficientNet was trained within sophisticated optimization and effectively extracts latent features from most image datasets, CAE is trained to fully reconstruct the input image. These vectors for reconstructing images seem to extract more precise latent features from the image within much fewer parameters than pre-trained vectors from a sophisticated model.

To demonstrate the benefit of searching similar maps to forecasters, we quantified the relation between the actual weather status of each searched similar date and that of the reference date. For the weather status, wind speed and wind direction were chosen because the wind itself has high relation with satellite images which represent the air pressure. Similarities of wind speed and wind direction of each date pair (reference date and similar date) were calculated by reference date and the similarities of all reference dates were averaged. Final averaged values were compared with the standard deviation of all samples. Similarity distance in wind speed was defined by the root mean squared error of the two speeds and similarity distance in wind direction was defined by the average difference between the angles of the two wind directions.

Table 5
Mean values, standard deviations of a year and calculated distances in wind speed (in m/s) and wind direction (in rad).

Weather status	Mean	Std.	Distance
Wind speed	1.892	0.1521	**0.0478**
Wind direction	2.231	0.4633	**0.1820**

As shown in Table 5, the distances in wind speed and wind direction of similar date pairs were lower than the standard deviation, which are 31.42 percent and 39.28 percent of the standard deviation respectively. The result indicates that the similarities in actual weather factors between the reference date and searched date were highly connected to the similarities between satellite images themselves. Thus, forecasters can access directly the satellite images of meteorologically related dates and utilize the past data in weather analysis procedures, which demands an empirical inference in the decision process.

5. Discussion

By comparing two latent vectors of weather maps using a convolutional autoencoder, Inception, and EfficientNet model, we could search similar weather maps of each day. The searched weather maps also showed high similarity in terms of several metrics used to measure the similarity of the two images. The models based on the convolutional neural network seem to capture the imagery features of weather maps considering the low relative error and the difference between RE_H and RE_T. RE_H was measured the same as RE in the test period which means the temperature image maps were not considered as major factors compared to the geopotential height images in the searching process. As shown in sample images from Figs. 4 to 6, the geopotential height images are more complex than the temperature images in the air pressure of 1000. The geopotential height is usually considered as a major factor when a human investigator searches the similar images and the experiment results also show meteorologically corresponding results, which indicates that the searching method used in this paper can assist the weather forecasters to search for similar images of a reference day.

6. Conclusion

To assist weather forecasting for weather forecasters, applying deep learning methods to find past weather maps similar

to current weather maps has been explored. Satellite images were converted into low dimensional vectors using a convolutional autoencoder and pre-trained convolutional neural network models. We listed the dates which are closely related to the reference date by comparing the Euclidean distances between the latent feature vectors of each date. The similarities of satellite images of searched dates to those of the reference date were measured using several metrics. The results showed that CAE extracted the features which are suitable for searching because it shows better performance than the previously learned model for the existing image classification.

Even though several metrics are used as a means of verifying similarity, similarity can ultimately vary according to the subjective judgment of an individual, and image similarity does not necessarily indicate meteorological similarity. To demonstrate the relation between searching similar satellite images and searching meteorologically similar dates, we compared similarity distances in actual weather factors including wind speed and wind direction of each date.

This study introduces a convolutional neural network approach to offer the list of meteorologically related dates to weather forecasters. Searching similar satellite images with an artificial intelligence model can help the forecasters efficiently access the records and conduct more empirical and precise analyses for current weather.

CRediT authorship contribution statement

Heewoong Ahn: Methodology, Investigation, Software, Formal analysis, Writing – original draft. **Sunhwa Lee:** Methodology, Investigation, Software, Formal analysis, Writing – original draft. **Hanseok Ko:** Supervision, Project administration, Writing – review & editing. **Meejoung Kim:** Supervision, Validation. **Sung Won Han:** Supervision, Conceptualization, Validation. **Junhee Seok:** Supervision, Conceptualization, Validation, Writing – review & editing.

Declaration of competing interest

The authors declare that they have no known competing financial interests or personal relationships that could have appeared to influence the work reported in this paper.

Acknowledgments

This research was supported by a grant from the National Research Foundation of Korea (NRF-2022R1A2C2004003) as well as a grant from Korea Meteorological Administration (Q171471). We thank KMA for assistance with this research and for providing ECMWF dataset.

References

[1] E.J. Timmermans, S. van der Pas, E.M. Dennison, S. Maggi, R. Peter, M.V. Castell, The influence of weather conditions on outdoor physical activity among older people with and without osteoarthritis in 6 European countries, J. Phys. Activity Health 13 (12) (2016) 1385–1395.

[2] S.A. Changnon, D. Changnon, E.R. Fosse, D.C. Hoganson, R.J. Roth Sr, J.M. Totsch, Effects of recent weather extremes on the insurance industry: major implications for the atmospheric sciences, Bull. Am. Meteorol. Soc. 78 (3) (1997) 425–436.

[3] M.D. Agnew, J.E. Thornes, The weather sensitivity of the UK food retail and distribution industry, Meteorol. Appl. 2 (2) (1995) 137–147.

[4] D.E. Hancher, H.A. Abd-Elkhalek, The effect of hot weather on construction labor productivity and costs, Cost Eng. 40 (4) (1998) 32.

[5] D.M. Ward, The effect of weather on grid systems and the reliability of electricity supply, Clim. Change 121 (1) (2013) 103–113.

[6] D. Scott, C. Lemieux, Weather and climate information for tourism, Procedia Environ. Sci. 1 (2010) 146–183.

[7] J.F. Thompson, R.G. Mutters, Effect of weather and rice moisture at harvest on milling quality of California medium-grain rice, Trans. ASABE 49 (2) (2006) 435–440.

[8] W.B. Beckwith, The effect of weather on the operations and economics of air transportation today, Bull. Am. Meteorol. Soc. 52 (9) (1971) 863–869.

[9] L.B. Lave, The value of better weather information to the raisin industry, Econometrica 31 (1–2) (1963) 151–164.

[10] A.H. Murphy, What is a good forecast? An essay on the nature of goodness in weather forecasting, Weather Forecast. 8 (2) (1993) 281–293.

[11] Kim, et al., Searching similar weather maps using principal component analysis and image pattern matching, Proc. Korean Meteorol. Soc. (2012) 62–63.

[12] Oh, et al., Searching past weather maps of East Asia using deep learning, Proc. Korean Meteorol. Soc. (2017) 741–742.

[13] A. Krizhevsky, I. Sutskever, G.E. Hinton, Imagenet classification with deep convolutional neural networks, in: Advances in Neural Information Processing Systems, 2012, pp. 1097–1105.

[14] Yi Sun, Xiaogang Wang, Xiaoou Tang, Deep learning face representation from predicting 10, 000 classes, in: Proceedings of the IEEE Conference on Computer Vision and Pattern Recognition, 2014, pp. 1891–1898.

[15] S. Lawrence, C.L. Giles, A.C. Tsoi, A.D. Back, Face recognition: A convolutional neural-network approach, IEEE Trans. Neural Netw. 8 (1) (1997) 98–113.

[16] N. Kalchbrenner, E. Grefenstette, P. Blunsom, A convolutional neural network for modelling sentences, 2014, arXiv preprint arXiv:1404.2188.

[17] Y. Jia, E. Shelhamer, J. Donahue, S. Karayev, J. Long, R. Girshick, T. Darrell, Caffe: Convolutional architecture for fast feature embedding, in: Proceedings of the 22nd ACM International Conference on Multimedia, ACM, 2014, pp. 675–678.

[18] Y. Chen, H. Jiang, C. Li, X. Jia, P. Ghamisi, Deep feature extraction and classification of hyperspectral images based on convolutional neural networks, IEEE Trans. Geosci. Remote Sens. 54 (10) (2016) 6232–6251.

[19] C. Szegedy, W. Liu, Y. Jia, P. Sermanet, S. Reed, D. Anguelov, Going deeper with convolutions, in: Proceedings of the IEEE Conference on Computer Vision and Pattern Recognition, 2015, pp. 1–9.

[20] C. Szegedy, V. Vanhoucke, S. Ioffe, J. Shlens, Z. Wojna, Rethinking the inception architecture for computer vision, in: Proceedings of the IEEE Conference on Computer Vision and Pattern Recognition, 2016, pp. 2818–2826.

[21] C. Szegedy, S. Ioffe, V. Vanhoucke, A. A. Alemi, Inception-v4, inception-resnet and the impact of residual connections on learning, in: Thirty-First AAAI Conference on Artificial Intelligence, 2017.

[22] TAN, Mingxing; LE, Quoc. Efficientnet: Rethinking model scaling for convolutional neural networks, in: International Conference on Machine Learning, PMLR, 2019, pp. 6105–6114.

[23] J. Masci, U. Meier, D. Cireşan, J. Schmidhuber, Stacked convolutional auto-encoders for hierarchical feature extraction, in: International Conference on Artificial Neural Networks, Springer, Berlin, Heidelberg, 2011, pp. 52–59.

[24] O.E. David, N.S. Netanyahu, Deeppainter: Painter classification using deep convolutional autoencoders, in: International Conference on Artificial Neural Networks, Springer, Cham, 2016, pp. 20–28.
[25] B. Girod, What's wrong with mean-squared error? Digit. Images Human Vis. (1993) 207–220.
[26] M.S. Charikar, Similarity estimation techniques from rounding algorithms, in: Proceedings of the Thiry-Fourth Annual ACM Symposium on Theory of Computing, ACM, 2002, pp. 380–388.
[27] H.V. Nguyen, L. Bai, Cosine similarity metric learning for face verification, in: Asian Conference on Computer Vision, Springer, Berlin, Heidelberg, 2010, pp. 709–720.
[28] Z. Wang, A.C. Bovik, H.R. Sheikh, E.P. Simoncelli, Image quality assessment: from error visibility to structural similarity, IEEE Trans. Image Process. 13 (4) (2004) 600–612.
[29] P.C. Teo, D.J. Heeger, Perceptual image distortion, in: Human Vision, Visual Processing, and Digital Display V, Vol. 2179, International Society for Optics and Photonics., 1994, pp. 127–142.
[30] Z. Wang, A.C. Bovik, L. Lu, Why is image quality assessment so difficult? in: ICASSP, Vol. 4, 2002, pp. 3313–3316.
[31] A.M. Eskicioglu, P.S. Fisher, S.Y. Chen, Image quality measures and their performance, 1994.
[32] I. Avcibaş, B. Sankur, K. Sayood, Statistical evaluation of image quality measures, J. Electron. Imaging 11 (2) (2002) 206–223.
[33] H.R. Sheikh, A.C. Bovik, Image information and visual quality, in: 2004 IEEE International Conference on Acoustics, Speech, and Signal Processing, Vol. 3, IEEE, 2004, pp. iii–709.
[34] D.P. Dee, S.M. Uppala, A.J. Simmons, P. Berrisford, P. Poli, S. Kobayashi, The ERA-Interim reanalysis: Configuration and performance of the data assimilation system, Q. J. R. Meteorol. Soc. 137 (656) (2011) 553–597.
[35] P. Berrisford, D.P.K.F. Dee, K. Fielding, M. Fuentes, P. Kallberg, S. Kobayashi, S. Uppala, The ERA-Interim Archive, ERA report series, (1) 2009, pp. 1–16.